



Removal of Malachite green and cadmium ions using nifty combination of metal functionalized graphene based composites from refuse dry cell batteries

Sofia Laraib*, Sana Zulfiqar

Department of Environmental Sciences (Chemistry), Fatima Jinnah Women University, Rawalpindi, Pakistan, emails: sofialaraib@gmail.com (S. Laraib), sanazulfiqar@fjwu.edu.pk (S. Zulfiqar)

Received 16 February 2021; Accepted 11 June 2021

ABSTRACT

The persistent use of toxic chemicals, that is, azo dyes and heavy metals in various sectors like industries, agriculture and research laboratories have resulted in polluting different compartments of the environment with the residues. The present communication specifically aims to synthesize a nifty combination of graphene oxide (GO) functionalized with metal particles, that is, silver (Ag) and copper (Cu) to remediate the pollutants from the wastewater using the adsorption process. GO functionalized with a silver (AgGO) and copper metal (CuGO) were synthesized respectively and characterized as adsorbents for the removal of Malachite green, cadmium ions (Cd^{2+}) and as a microbial entity, that is, *Staphylococcus aureus*. Results of Fourier-transform infrared spectroscopy and X-ray fluorescence techniques have confirmed the synthesis of GO and its functionalization. A close batch system of 60 min was designed to study the adsorption process under various parameters (concentration, contact time) using ultraviolet-visible spectroscopy and flame atomic absorption spectroscopy. Comparison of percentage removal of heavy metal between composites revealed a better adsorption trend by AgGO (94%) as compared with the prepared CuGO (84%) from wastewater. Contrary to that the percentage removal of azo dyes is 98% by CuGO. Kinetic studies favored pseudo-second-order and intraparticle diffusion models whereas adsorption studies favored Langmuir and Freundlich isotherms. The proposed composite comprises of graphene which is labeled as a bactericidal agent and after its metal functionalization enhances the antibacterial activity marvelously.

Keywords: Graphene oxide; Dry cell batteries; Silver and copper metal particles; Anti-bacterial assay; Wastewater treatment

1. Introduction

Nature has the capacity to host several complex and dynamic ecosystems and every major ecosystem faces threats at different time periods due to unsustainable developments. The 21st century is an era that concerns too much about the environment while environmental pollution and its remediation are the craving issue of this century [1,2]. Environmental challenges are accelerating because of exploding human population and competing for interest in the usage of advanced systems, resultant in posing greater demand pressure on existing natural resources. Thus, the

increase of demands accelerates the rate of environmental deterioration through depletion of resources, disruption of the natural environment, and increasing pollution. On the other hand, ensuring the basic requirements, that is, food, drinking water, energy, shelter, etc. without compromising the future needs is one of the pressing issues faced worldwide [3]. These challenges cannot be clearly defined, either their solutions cannot be fitted into a neat box so requires a group of individuals, regional, national and international level solutions to resolve the problems [4].

According to World Bank 3,900 million m^3 of freshwater is consumed annually, comprising of agriculture (60%),

* Corresponding author.

industrial wastewater (22%) and domestic (18%), in 2014 (latest update data) [5].

According to WHO, almost half of the world's population will be living in water-scarce areas by 2025. According to a study conducted by the International Monetary Fund (IMF), Pakistan is the third on the list of countries that are facing a serious water crisis. Pakistan Council of Research in Water Resources (PCRWR) announced in May 2018, that very little or no clean water will be available by 2025, in the country. Currently, clean drinking water can be accessed by only 20% of the country's population. The remaining 80% population relies on polluted water contaminated with fertilizer, pesticides, and industrial contaminants such as heavy metals and dyes. Around 80% of all diseases and 30% of deaths are a consequence of such water pollution [6].

A major threat to public health in Pakistan is due to water pollution. Water quality is not properly monitored in Pakistan and Pakistan ranks 80th out of 122 nations in maintaining water quality standards [7]. Both water scarcity and pollution pose a major threat to human existence and eco system's health around the globe. Furthermore, the overwhelming increase in agricultural and industrial activities is responsible for the innumerable release of a variety of anthropogenic pollutants such as organic pollutants, heavy metals, and dyes into the aquatic environment, causing a significant addition to this global issue [8].

There is a need for management and conservation approaches impaired with the newer technologies that can be derived from applied research for satisfying humankind's demands in a sustainable way [9]. In the past couple of decades, scientists tend to focus on remediation of pollutants and their control techniques and significant researches have been done to explore the abilities of solid-phase adsorbent materials for the removal of unwanted components from the environment and have succeeded to a large extent [10].

A variety of pollutants are responsible for contaminating natural water resources such as infectious agents, organic pollutants, inorganic pollutants and oxygen demanding waste [11]. Among various pollutants, organic dyes and heavy metals are categorized as the most momentous water pollutants since they are non-biodegradable, carcinogenic, and are highly toxic [12].

Metals and dyes released through these sources get in to the food web, their mutual effects cause a series of damage to the health of living organisms which is so often irreversible [13].

The presence of heavy metals in the drinking water of District Buner was evaluated by a scientist in literature [14]. For this research presence of heavy metals such as Ni, Zn, Pb, Cr, and Cd in both ground and surface water in the District Buner (Pakistan) were determined and the obtained results were compared with their safe limits prescribed by Pakistan Environmental Protection Agency (Pak-EPA) and WHO. In the study area, the majority of the drinking water samples exceeded the safe limit of Pak-EPA and WHO. The result showed that Cr, Pb, and Cd were significantly higher as compared to Pak-EPA and WHO. These high concentrations of heavy metals in the study area may be due to mafic and ultramafic rocks, marble industries, mining, smelting, and intensive agricultural practices.

Various operations of textile industries result in the release of billions of gallons of wastewater that carries a variety of toxic dyes and pigments. Annually around 7 lakh tons of more than 10,000 types of pigments and dyes are used worldwide and 10%–15% of this volume is disposed of as wastewater without any treatment. Synthetic dyes are non-biodegradable molecules that contain the main residue existing in the waste coming out of the dyeing industry. Acute toxicity tests exposed that various synthetic dyes are not predominantly lethal. Yet, their perseverance and long exposure time is of great apprehension, since these substances lead to long-lasting effects such as mutagenic impairment and carcinogenicity to living organisms [15].

A number of treatment methods are used for the polluted water [16] which mainly includes sorption [17–19], chemical precipitation [20,21], membrane filtration [22,23], ion exchange [24,25], and coagulation [26,27].

Conventional methods for polluted water remediation are becoming inadequate and reasons behind their less efficiency include high cost, toxic by-product formation, the requirement of high effort, energy and toxicity [28]. Considering the persistent presence and toxicity of Malachite green (MG) dye and Cd^{2+} ions in water bodies of Pakistan, several researchers have synthesized competent adsorbent materials like chitosan and hydroxyapatite-based adsorbents [6]. Similarly, wheat bran and neem sawdust was being studied for the removal of Malachite green with maximum dye removal of 90% and 75.78% respectively [29]. Another promising adsorbent synthesized from waste chicken eggshells was used as an adsorbent for the removal of Cadmium (Cd) heavy metal in an aqueous solution. Results showed that waste chicken eggshells as adsorbent represents a good removal strategy, that is, 73.42% but such adsorbents could not be used on large scale due to limited availability and high price [30]. Researchers conducted so far on the efficiency of multi-walled carbon nanotubes and powdered activated carbon also predicted less adsorption potential as compared to graphene and its oxides as adsorbents.

Graphene is one of the attractive stuff now a day due to its easier processing, and its significance of having oxygen moieties attached on its surface is quite attractive to grow chemical structures on its surface [31]. Graphene oxide (GO) is titled as the next generation material due to the marvelous properties that make it an outstanding material among various other adsorbents studied so far, that is, hydroxyapatite and chitosan [32]. Graphene is comprised of sp^2 -hybridized carbon atoms arranged in a two-dimensional honeycomb lattice. The highly negative charge density on the surface of graphene makes it a promising moiety for capturing cationic pollutants from aqueous mediums. Although GO is a promising adsorbent material but its ability to make stable collides hinders the efficient recovery of adsorbent [33]. However, the use of metals to immobile GO provides an opportunity to synthesize composite materials with nifty properties for phase separation and adsorption. To this end, functionalized GO-based materials have been analyzed extensively for adsorption applications due to their good chemical stability, structural diversity, low density and suitability for large-scale production [34]. Their textural properties, such as average pore diameter,

total pore volume and infinitely high surface-to-volume ratio, have stimulated a large number of investigations as potential adsorbents for water purification and for biological applications [35]. GO usage has been reported in various studies, ranging from adsorption of metal ions, electrochemical sensors to detect trace level lead [36], biosensors [37], electrodes for supercapacitors, and batteries [38]. Researches have also assessed a comparison among graphene, metal and graphene oxide, nanocomposites and graphene functionalized with organic compounds for removal of different pollutants from water because of their increased efficiency and selectivity [38]. In another study conducted by a scientist in literature [28], graphene oxide and polydopamine composites can be synthesized and its adsorption capacity can be evaluated for two dyes; Nile blue and Paraquat from wastewater. Results revealed that this composite has an adsorption capacity of 131.58 mg g⁻¹ for Nile blue and 101.01 mg g⁻¹ for Paraquat respectively.

Herein, suitable adsorbents from GO have been synthesized by utilizing refused dry battery cells as a source of graphite, for the removal of noxious pollutants (MG, Cd²⁺) from wastewater. Moreover, this nifty combination of metal and GO synthesized using facile cross-linking methodology will be cost-effective, eco-friendly along with excellent antimicrobial properties that will help in wastewater remediation even from pathogenic bacterial.

2. Experimental

All reagents used were of analytical grade and were purchased from Sigma-Aldrich (UK) and Merck (Germany).

2.1. Chemicals and reagents

Hydrochloric acid (HCl) 37%, hydrogen peroxide (H₂O₂) 30%, sulfuric acid (H₂SO₄) 95.98%, ammonia solution 25% were purchased from Sigma-Aldrich (USA). Sodium nitrate (NaNO₃), glucose (C₆H₁₂O₆), silver sulfate (Ag₂SO₄), copper sulfate pentahydrate (CuSO₄·5H₂O) and potassium permanganate (KMnO₄) were purchased from Riedel-de Haën (Germany). Mannitol Salt Agar (MSA) and Mueller Hinton Agar (MHA) were purchased from Bio World (USA) and Merck (USA) respectively. All the chemicals were of analytical reagent grades and used as received, without further purifications. The aqueous solutions were prepared in distilled water. Refuse dry cells (AA type batteries) of Sony and Toshiba were used for graphite extraction.

2.2. Synthesis of graphene oxide

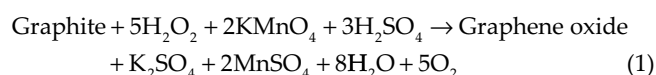
2.2.1. Graphite extraction

Graphite was extracted from graphite rods (8 mm in diameter and 5.8 cm in length) of refused dry cells (Sony and Toshiba) and was placed in sunlight. Silicon Carbide Paper was used for scrapping to remove all kinds of electrolytic paste attached to them. Swilling of scrapped graphite rods was done in a sonicator bath (35°C, 10–15 min) and subjected to etching treatment (0.6 M HCl, 0.5 h). It was then exposed to the repeated cycles of rinsing with acetone, oven-dried and crushed into fine powder [39,40].

2.2.2. Graphene oxide formation

The synthesis of GO was done by following the modified Hummers Method with few revisions [41–43]. Overall synthesis was done in several steps. In the first step, exfoliation of graphite was done by mixing graphite (2 g) in 98% H₂SO₄. The reaction temperature (2°C–5°C) was controlled by giving ice treatment for consecutive 4 h followed by the slow addition of 12 g of KMnO₄ which increase its temperature up to 15°C. So in order to maintain temperature further icing was done till 30 min. As a result, a brownish slurry-like crude product (GO) was obtained which was further diluted with 200 mL of distilled water under rigorous stirring (2 h). In the second step, this product was further purified under reflux at various temperatures (98°C for 20 min then 30°C for 15 min followed by 25°C for 2 h) followed by 30 mL H₂O₂ addition in two separate beakers, resting it overnight. Prepared GO was centrifuged with the solution of 10% HCl, followed by successive washing until pH becomes neutral (Fig. 1) [Eq. (1)]. In the third step, the resultant gel-like GO was vacuum dried (80 kPa, 9 h), ground and kept in Desiccator until further use [44] as shown in Fig. 1. NaNO₃ was excluded from the synthesis process considering the environmental aspects, that is, harmful emissions of NO_x [45,46].

Overall reaction of GO formation:



2.2.3. Graphene oxide functionalization

Prepared GO (2 g) was further functionalized in order to enhance its adsorption properties. For this purpose, GO solution was prepared in 2,000 mL deionized water under ultrasonication. In stabilization of the solution was done with the addition of glucose 90 g under rigorous stirring. In a separate beaker, silver sulfate along with ammonia solution (0.55 mol L⁻¹) was added for smooth dissolution. Both the solutions GO and Ag(SO₄)₂ were mixed together and then placed aside (3 h) after stirring of 1 h. The resultant functionalized graphene oxide was settled down at the bottom of the beaker. The supernatant was poured out and the leftover brownish product was purified by repeated cycles of washing before drying in a vacuum Desiccator [47]. The sample coded as AgGO.

Following the same methodology, GO was also functionalized with copper sulfate pentahydrate (CuSO₄·5H₂O) and the resultant sample (Fig. 2) was coded as CuGO [48,49].

2.3. Isolation of *Staphylococcus aureus* gram-negative strain

Antibacterial properties assessment of prepared products GO, AgGO, CuGO was done as follows. MSA, MHA and brine solution (100 mL) were prepared and autoclaved. Petri plates (90 mm) were treated under a UV lamp (10–15 min) and both agars (55°C) were then poured into those Petri plates. The gram-negative strain of *Staphylococcus aureus* was isolated from Nullah Lai wastewater using series of dilutions (dilution factor 10⁶) and was further streaked

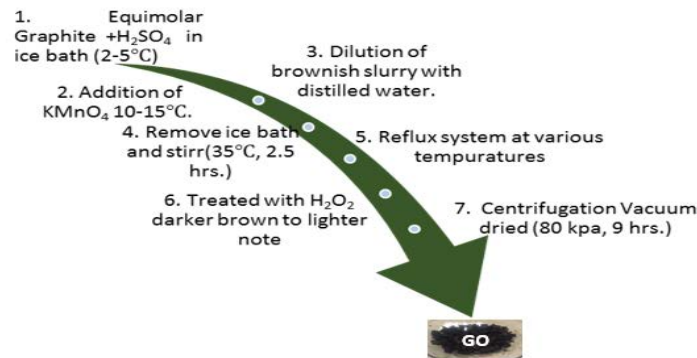


Fig. 1. Synthesis of GO.

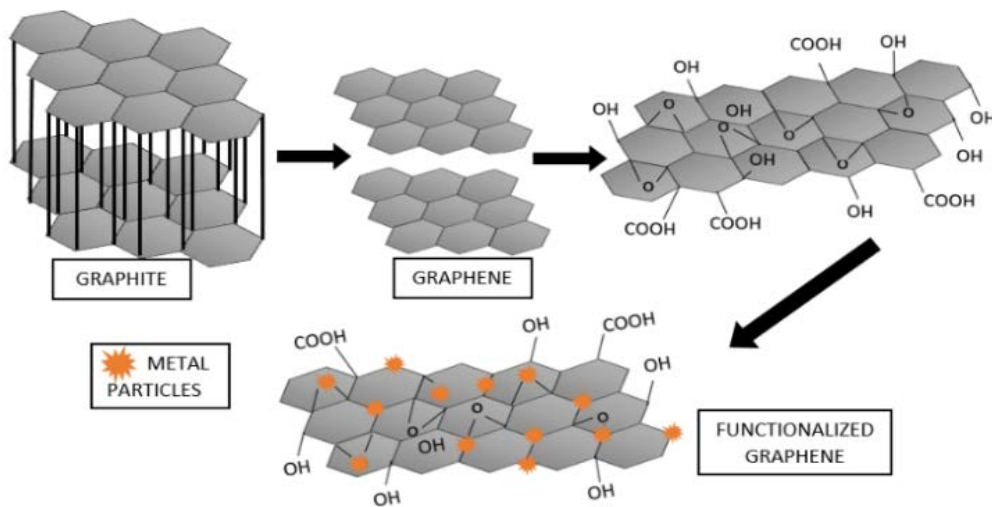


Fig. 2. Schematic representation of functionalization process of GO.

on the MSA agar plates. Streaked plates were incubated (24–48 h, 35°C–37°C) and resultant colonies of *Staphylococcus aureus* were isolated (Fig. 3) and restreaked onto the MSA agar plates to have a lawn of *Staphylococcus aureus* [50].

2.4. Catalase test

This test was conducted for the confirmation of the bacteria *Staphylococcus aureus* species. The isolated bacterial inoculum was placed on a sterile glass slide and 2 drops of hydrogen peroxide (H₂O₂) were dripping. Inoculum started bubbling due to the formation of oxygen gas as a result of activity by catalase enzyme specific to this bacterial strain [51] (Fig. S1). Eq. (2) shows the overall reaction.



2.5. Disk diffusion method

Whatman Filter paper discs were prepared (10 mm each) and sterilized by placing under a UV lamp (10 min). The prepared discs were impregnated with the composite solutions (0.5 mL) and let dry. The filter paper discs were then placed on *Staphylococcus aureus* streaked MHA agar plates

and incubated (24 h) without inversion. Inhibition zones of different diameters were observed around the discs and were measured by measuring scale [52].

2.6. Adsorption isotherms

Adsorption isotherm describes how the solute particles interact with the adsorbent and assesses the distribution of a solute between the solid and the liquid phase by measuring the distribution coefficient. To assume whether the adsorption process was a single layer or multilayer phenomenon several models are applied as discussed below. The linear expression used to calculate Langmuir isotherms is expressed by Eq. (3):

$$\frac{C_e}{q_e} = \frac{1}{q_{\max} K_L} + \left(\frac{1}{q_{\max}} \right) C_e \quad (3)$$

where C_e (mg L⁻¹) is the equilibrium concentration of adsorbate, q_e (mg g⁻¹) is the amount of adsorbate adsorbed per unit mass of adsorbent, and q_{\max} (mg g⁻¹) and K_L (L mg⁻¹) are the Langmuir constants related to maximum monolayer adsorption capacity and energy change in

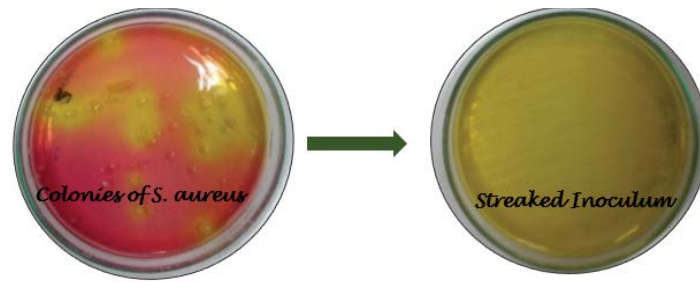


Fig. 3. Microbial isolation.

adsorption. Eq. (4) is the Freundlich equation used to calculate adsorption capacity.

$$\log q_e = \log K_F + \left(\frac{1}{n}\right) \log C_e \quad (4)$$

where C_e (mg L^{-1}) is the equilibrium concentration of the adsorbate, q_e (mg g^{-1}) is the amount of adsorbate adsorbed per unit mass of adsorbent, and K_F and n are Freundlich constants, K_F is the adsorption capacity of adsorbent and n is an indicator adsorption process. Adsorption kinetics experiments were conducted to investigate the effect of contact time, to obtain the resulting kinetic parameters and to represent the adsorption reaction. The fitted conventional models of adsorption reaction are pseudo-first-order rate, pseudo-second-order rate and intraparticle diffusion model. Pseudo-first-order rate can be expressed by Eq. (5), that is,

$$\log(q_e - q_t) = \log q_e - k_1 t \quad (5)$$

where q_e and q_t is the amount of adsorbate adsorbed at equilibrium and at time t , k_1 is the overall rate constant of the reaction. Eq. (6) is describing the pseudo-second-order rate:

$$\frac{t}{q_t} = \frac{1}{k_2 q_e^2} + \frac{1}{q_e t} \quad (6)$$

where k_1 (min^{-1}) and k_2 ($\text{g mg}^{-1} \text{min}^{-1}$) are constants of adsorption rate, q_t (mg g^{-1}) is adsorption capacity at time t (min), q_e is adsorption capacity at equilibrium conditions (mg g^{-1}). To suggest the slow step involved in the adsorption process the kinetics data is subjected to Boyd kinetics model analysis [Eq. (7)].

$$B_t = -0.4977 - \ln(1 - F) \quad (7)$$

where F represents the fraction of solute adsorbed at any time, t (min), as calculated from $F = q_t/q_e$. Whereas, intraparticle diffusion model [Eq. (8)] empirically noted that uptake varies almost proportionally with $t^{1/2}$ rather than with the contact time, t , according to this theory,

$$q_t = k_i \sqrt{t} + C_i \quad (8)$$

where k_i ($\text{mg g}^{-1} \text{min}^{-1}$) is intraparticle diffusion constant C_i is the constant which describes the boundary layer effect. In this research, R^2 values are high which means the intraparticle diffusion model plays an important role in the adsorption process [53,54].

3. Characterization techniques

Characterization techniques used were Fourier-transform infrared spectrophotometer (FTIR-8400 Shimadzu, Japan) and X-ray fluorescence spectroscopy (XRF-HITACHI X-MET8000 Expert Geo). The former technique was employed to identify organic functional group linkages in synthesized graphite composites within the transmittance range of 400–4,000 while the latter technique was used as a non-destructive analytical technique with an elemental range from Mg-U respectively. The calibration selected for the analysis was ALLOY-LE-FP.

4. Schematic layout of synthesized composites and its applications

Fig. 4 is the graphical layout displaying the overall synthesis of GO, its functionalization with metals and their application for the removal of dye (MG), metal ions (Cd^{2+}) and anti-microbial affinity.

5. Results and discussion

5.1. FTIR spectroscopy

All the synthesized samples are analyzed by FTIR and the spectra reveal that $\text{C}\equiv\text{C}$ is attributed to the inherent chemical bonding in graphite and noteworthy changes in O–H and $\text{C}=\text{C}$ stretching peaks is attributed to the successful in-situ wedging process (Hummer's Method) of graphite [55] (Figs. S2–S5). Stretching of the carbon bonds as shown in FTIR spectra of GO(c) are actually providing room for the attachment of Ag and Cu metal particles (Fig. 5) by means of a covalent coupling or electrostatic interaction [56].

Peaks at $1,386 \text{ cm}^{-1}$ of GO(c) is corresponding to the dimeric COOH groups attached by hydrogen bonding to the hydroxyl group [57]. All the O–H groups present in the proximal vicinity of graphite have the tendency of being hydrogen-bonded, and their cumulative intensity results in a deeper and broader OH peak. The broad stretching peaks around $\sim 3,700$ to $3,000 \text{ cm}^{-1}$ are the hydroxyl groups

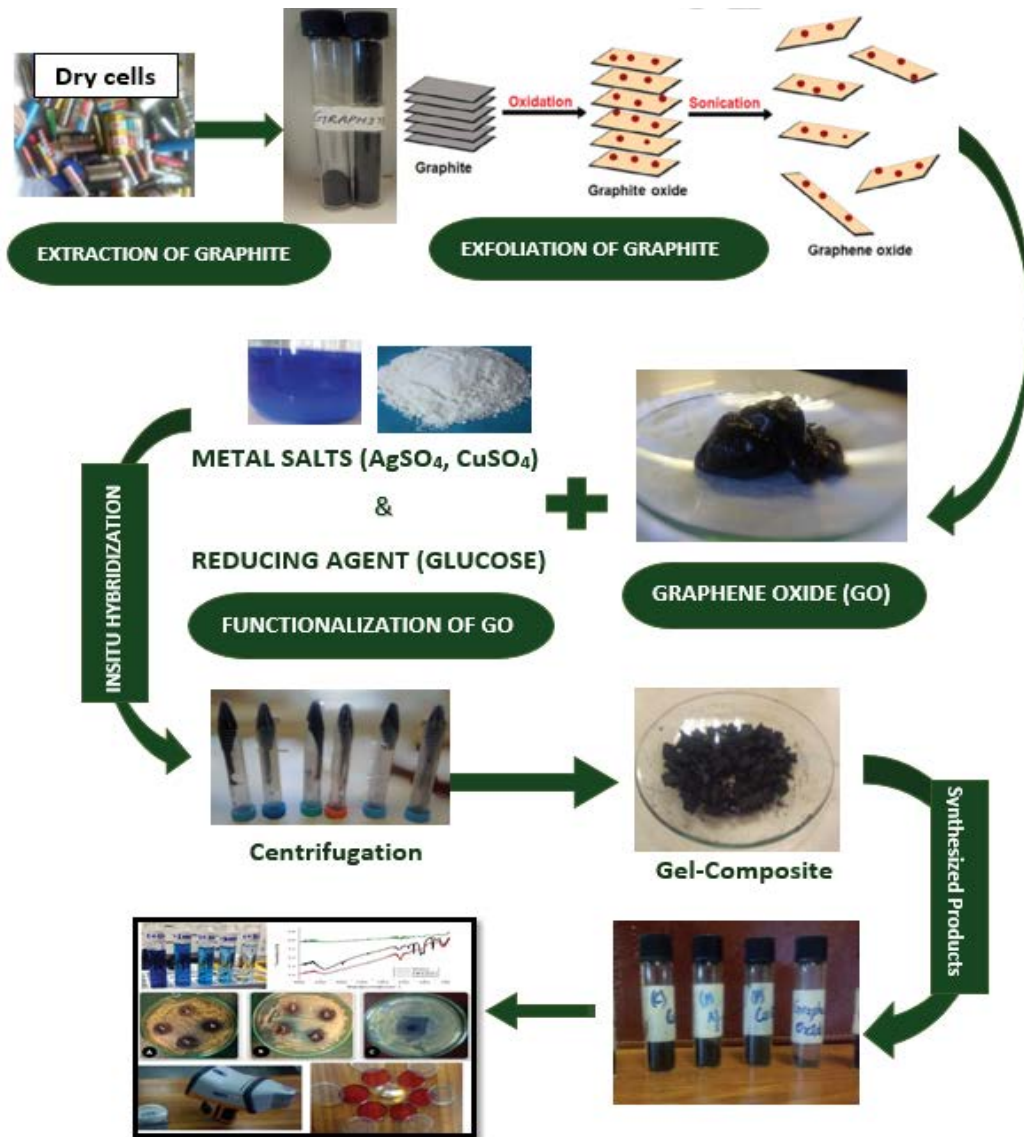


Fig. 4. Graphical layout.

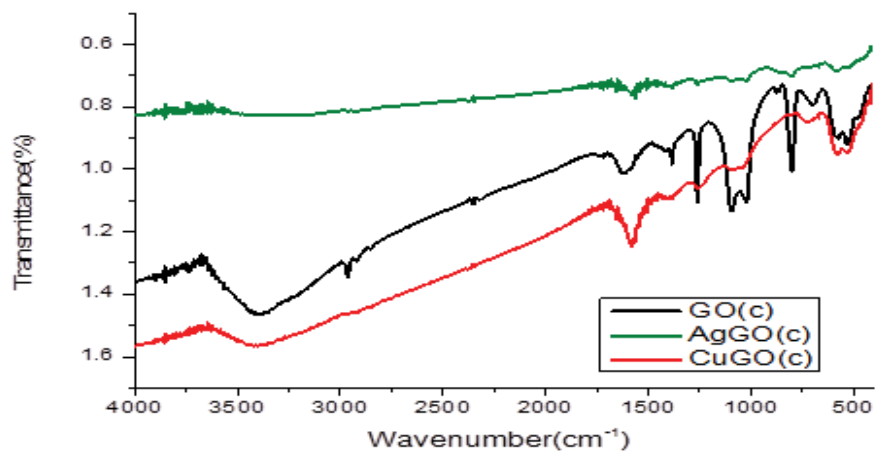


Fig. 5. FTIR spectra of GO(c) and its composites.

demonstrating the absorbed water molecules, OH from carboxylic groups or phenolic OH of GO [58,59] as shown in Fig. 5. These are the fundamental spectral changes that ensure the widespread oxidation of graphitic structure into graphene oxide [60].

The spectra of synthesized composites show a noteworthy decreasing trend in the sharpness and broadness of hydroxyl peaks as compared to that of precursors, that is, GO(c). It can be attributed to a higher concentration of metal ions due to functionalization, which replaced the hydroxyl group and get attached to the vacant sites thus decreasing the broadness of OH peaks [61].

5.2. XRF spectroscopy

The results obtained by XRF spectroscopy ensure the formation of the desired compound and are discussed as follows.

The presence of higher percentages of Mn in sample GO(c) is attributed to the addition of KMnO_4 during the exfoliation process that got subsequent reduction when GO(c) undergo metal functionalization [62,63].

The higher percentage of Cu in sample CuGO(c) shows the functionalization of graphene oxide with Cu metal. No sulfates were detected in the analysis of this sample which depicts that the Cu metal is get attached to the GO leaving sulfates in the supernatant layer [64,65].

The higher percentage of Ag in sample AgGO(c) shows the functionalization of graphene oxide with Ag metal (Table S1). No sulfates were detected in the analysis of this sample which depicts that the Ag metal is get attached to the GO leaving sulfates in the supernatant layer [66,67].

5.3. Scanning electron microscopy characterization

The microstructure of GO synthesized from graphite is observed with scanning electron microscopy (SEM) at magnifications of X20 as shown in Fig. 6. It is observed that particle size reduction has a significant effect on GO. As observed, the splitting of graphite stacks into layers is evident. The layers within the layer are further disassembled and a more crumpled structure is observed. This is the consequence of surface area (due to particle size reduction) that allows efficient oxidation and amorphization during the process as well as decreases the crystallinity of GO [68].

5.4. Adsorption studies

Adsorption studies as a function of time and initial concentration are considered to elucidate the adsorption phenomena. A close batch experimental system of 60 min with a time-lapse of 5 min is designed for the removal of dye and metal ions (MG and Cd^{2+} ions). Effect of different parameters, that is, time and initial concentration are studied while keeping the adsorbent dose (20 mg) constant.

For studying varying parameters stock solution of adsorbate is prepared in 500 mL distilled water. Aliquot of 0.01, 0.03, and 0.05 ppm and 0.1, 0.3 and 0.5 ppm of MG and Cd^{2+} respectively are taken separately. All the experiments are performed twice and are characterized using UV-Vis spectrophotometer (UV-1601 Shimadzu, Japan) and flame

atomic absorption spectrophotometer (Shimadzu, Model-A7000F, Japan). The removal percentage of pollutants and adsorption capacity has been studied using Eqs. (9) and (10), respectively.

$$\% \text{Removal} = \frac{C_i - C_t}{C_i} \quad (9)$$

$$q_{\max} = \frac{C_i - C_f}{m} \times V \quad (10)$$

where C_i and C_f are the initial and final concentrations of adsorbate ions (mg L^{-1}), V is the volume of adsorbate (L) and m is the mass of adsorbent (g). All experiments were carried out in duplicate and the mean values of q_e were reported. Standard derivation was deduced for each experimental system by using the following formula:

$$\text{S.D.} = \sqrt{\frac{\sum (x - \bar{x})^2}{n - 1}} \quad (11)$$

where \bar{x} is the sample mean (number 1, number 2) and n is the sample size.

5.4.1. Batch studies for the removal of azo dyes

The average active equilibrium for the dye (MG) is recorded between the time intervals of 40–55 min. The best composite for the removal of MG at all the concentrations, that is, 0.01, 0.03 and 0.05 ppm is CuGO(c) with the %R value of 98%, 82%, and 78% respectively. Eq. (12) shows the sequence showing the capability of composites for the removal of Malachite green.

$$\text{CuGO(c)98\%} > \text{AgGO(c)89\%} \quad (12)$$

5.4.1.1. As a function of time

There are many factors that are attributed to the variations in the equilibrium interval of the adsorbents (AgGO, CuGO). Mainly the porosity of the adsorbent, as well as the number of available binding sites, play the role of valuable factors that governs the phenomena of adsorption [69]. As the contact time increases, more adsorbate molecules (MG dye) are subjected to the available vacant sites of adsorbent and after attaining the dynamic equilibrium there is usually a decrease in the removal efficiency because an increase in the contact time leads to the saturation of available active binding sites causing a repulsive tension among the molecules of adsorbate and adsorbent for the transfer of molecules (Fig. 7) [70]. The adsorption in graphene oxide is endothermic basically due to $-\text{OH}$ sites that support the hydrophobic interaction as stated in the literature [71].

5.4.1.2. As a function of initial concentration

The finding of the experiment shows that the %R is inversely related with the initial concentration of the adsorbate (MG dye), so the removal efficiency showed a decreasing trend with the increase in the initial concentration

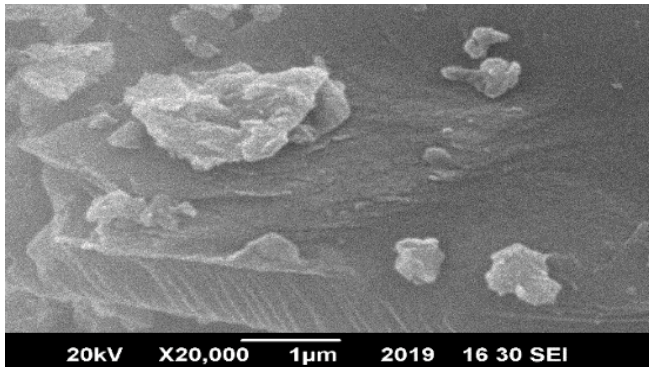


Fig. 6. SEM image of graphene oxide (GO).

of the MG dye, that is, %R is highest at 0.01 ppm and lowest at 0.05 ppm. This decreasing trend can be due to the unavailability of active binding sites of adsorbents (AgGO, CuGO) [72].

5.4.2. Comparison of adsorption trends of both (cationic and anionic) dyes

Batch analysis of GO(c) was carried out for the predicting removal percentage with both dyes. The CuGO composite showed a 98% removal percentage for MG as compared to Congo red (32%) respectively. The same adsorption trend was observed throughout the batch experiments (%R of MG > %R of CR) because GO has good adsorption capability due to the presence of hydrophilic sites on its surface [73]. It can be noted that with the addition of capping agents like metals, the adsorption capacity, as well as the retrieval capability of the adsorbent, is increased tenth folds as compared to GO from the sample solution due to its hydrophilic exterior and hydrophobic interior surface.

The functionalized GO was compared with various other adsorbents in cited literature [74]. Results supported functionalized GO as a good adsorbent of cationic dyes as compared to anionic dye (CR) [75,76].

5.4.3. Batch studies for the removal of heavy metals

Similarly, the functionalized GO was also used as an adsorbent for Cd^{2+} removal as a lab-based application. The dynamic equilibrium for adsorptive removal of Cd^{2+} metal ions was observed between the time interval of 40–55 min. The best removal of Cd^{2+} metal ions is done by AgGO(c) at all concentrations, that is, 0.1, 0.3 and 0.5 ppm with the removal efficiency of 94%, 82% and 72% respectively (Fig. 7). Eq. (13) shows the adsorptive trend for the removal of Cd^{2+} ions.

$$\text{AgGO(c)}\ 94\% > \text{CuGO(c)}\ 84\% \quad (13)$$

5.4.3.1. As a function of time

The adsorption experiment was conducted as a function of time. Results showed that as the contact time increases, the exposure of Cd^{2+} metal ions to the active binding sites of the composites also increases. The %R always increases with the increase in contact time till the equilibrium point, also supported by a literature review [2].

5.4.3.2. As a function of initial concentration

An adsorption experiment was also conducted as a function of concentration. Results (Fig. 8) showed that the removal efficiency is in inverse relation with the initial concentration so that the removal efficiency decreases with the increase in the initial concentration of the adsorbate (Cd^{2+} metal ions).

It can be seen from Fig. 8, the removal efficiency of functionalized GO is maximum at 0.1 ppm while at 0.3 and 0.5 ppm, a gradually decreasing trend is observed which is attributed to the saturation of active binding sites and the availability of limited pores of adsorbent (AgGO, CuGO). The number of binding sites and the porosity of the adsorbent depends upon the structure and chemical composition of the synthesized product [77].

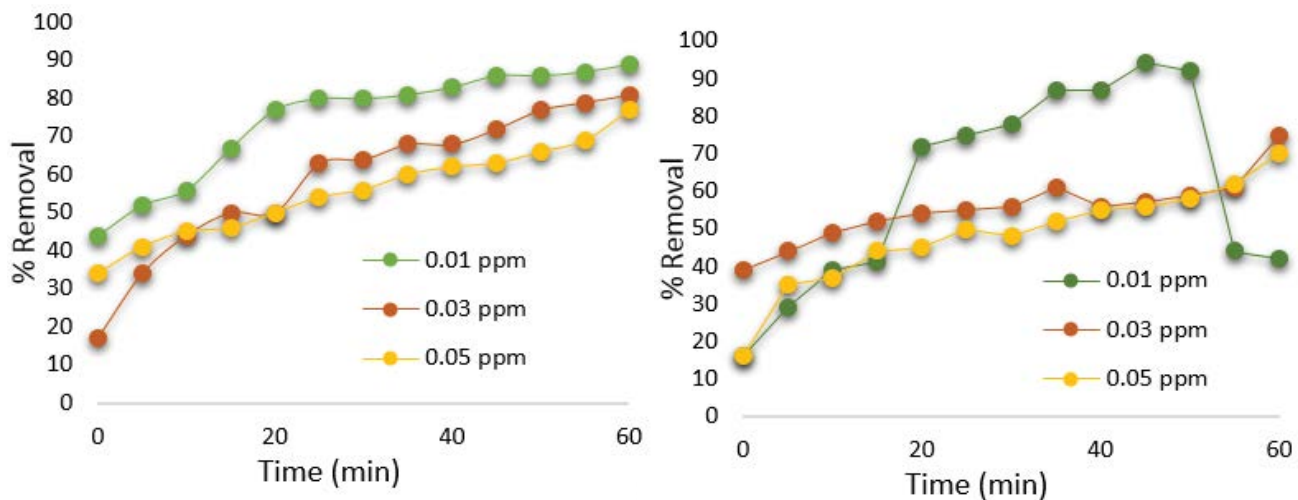


Fig. 7. Effect of time on the adsorption of Malachite green by (a) AgGO(c) and (B) CuGO(c).

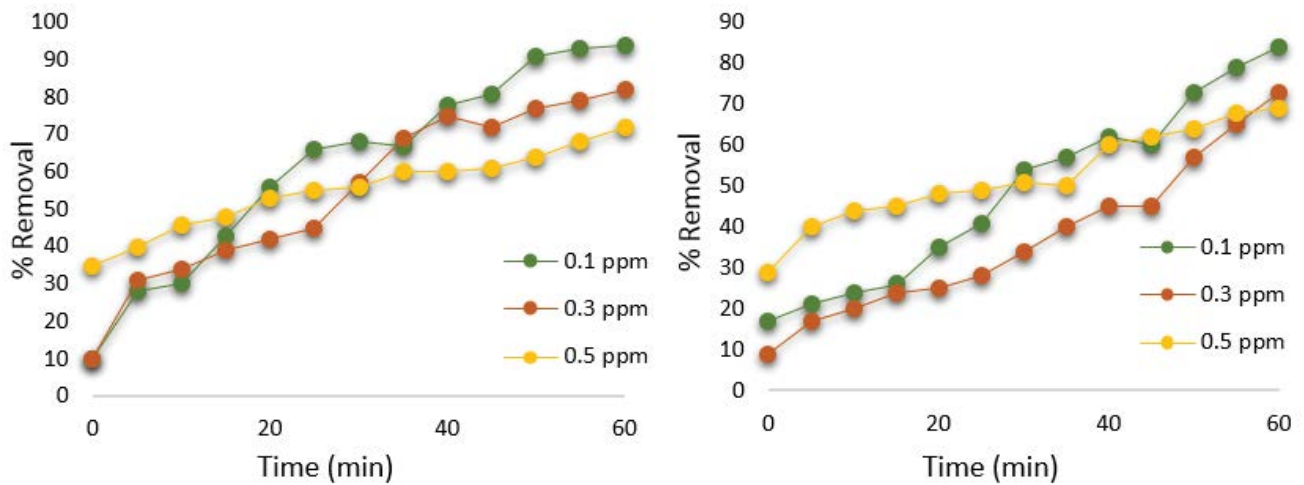


Fig. 8. Effect of time on the adsorption of Cd by (a) AgGO(c) and (b) CuGO(c).

5.4.4. Standard derivation

Standard derivations of all the adsorption processes towards MG and Cd^{2+} are calculated and reported in Table 1. The percentage removal is highly significant and lies within the range of 0.08–0.2 using the Excel tool.

5.5. Antibacterial susceptibility test

The anti-bacterial properties of GO and its functionalized composites (AgGO, CuGO) was also analyzed. Results showed that the measurements of inhibition zones recorded for GO are within the scale and thus, approving the anti-bacterial properties of GO in comparison to functionalized GO due to synergistic effects for the susceptibility for bacterial species as summarized in Table 2 (Fig. S6). Although the exact mechanism of antibacterial effects of GO and synthesized adsorbents has not been entirely clarified and various antibacterial actions have been proposed.

Owing to electrostatic attraction and affinity to sulfur proteins, GO and modified GO can adhere to the cell wall as well as the cytoplasmic membrane of *Staphylococcus aureus*. The adhered ions can enhance the permeability of the cytoplasmic membrane and lead to disruption of the bacterial envelope. This uptake may lead to the deactivation of respiratory enzymes and interrupt the functioning of adenosine triphosphate-ATP production by generating reactive species resulting in the provocation of cell membrane disruption and deoxyribonucleic acid (DNA) modification [78].

5.6. Adsorption isotherms and kinetics

Adsorption isotherms determine the distribution pattern of the molecules among the solid and liquid phases whenever they are subjected to adsorption specifically at the interval of dynamic equilibrium. The surface chemistry and the affinities of the synthesized adsorbents were insight by using renowned adsorption models proposed by Langmuir, Freundlich, intraparticle diffusion model and Byod plot.

Table 1
Standard derivations of all adsorption systems

Adsorbents	Concentrations (ppm)	%R	Standard derivation
AgGO(c)-MG	0.01	88	0.084
	0.03	81	0.261
	0.05	76	0.265
CuGO(c)-MG	0.01	98	0.034
	0.03	82	0.100
	0.05	78	0.271
AgGO(c)- Cd^{2+}	0.1	94	0.027
	0.3	82	0.065
	0.5	72	0.052
CuGO(c)- Cd^{2+}	0.1	84	0.083
	0.3	73	0.058
	0.5	69	0.057

Table 2
Anti-bacterial assessment results

No.	Synthesized adsorbent	Inhibition zone measurement (mm)
1.	GO	15
2.	AgGO	26
3.	CuGO	20

The models were applied to determine the best fitness of experimental data and to access the thermodynamics of the adsorption process [79].

Various parameters such as k_2 , q_e and R^2 were calculated for studying the best fitness approach of experimental data with applied models. It is evident from the summarized results in Table 3 that Langmuir and Freundlich isotherm models seem to be very well fitted with the value of regression coefficient >0.9 ensuring single as well as multi-layer

Table 3
Summarized results of adsorption models and kinetics

Models	Parameters	Malachite green		Cadmium	
		AgGO(c)	CuGO(c)	AgGO(c)	CuGO(c)
Langmuir model	q_{\max} (mg g ⁻¹)	8.92	8.08	2.10	3.24
	K_L (μg ⁻¹)	0.30	0.70	0.08	0.40
	R^2	0.82	0.99	0.96	0.95
Freundlich model	K_F (mg g ⁻¹)/(mg L ⁻¹) ^{1/n}	-0.15	-0.37	-0.22	-0.55
	1/n	2.18	1.61	1.23	1.27
	R^2	0.94	0.99	0.90	1
Pseudo-first-order	R^2	0.84	0.93	0.94	0.93
Pseudo-second-order	R^2	0.99	0.70	1	0.70
Boyd model	R^2	0.77	0.30	0.83	0.83
Intraparticle diffusion model	K_{id} (mg g ⁻¹ min ⁻¹)	0.02	0.04	0.010	0.013

adsorption trend [80] (Figs. S7 and S8). The regression coefficient of Boyd plots confirms that the adsorption mechanism is governed by external mass transport where adsorbate ions travel within the pores of the adsorbent excluding a small amount of adsorption that occurs on the exterior surface of the adsorbents (AgGO, CuGO) [81] (Fig. S9).

Kinetic studies is carried out by studying pseudo first and second order kinetic models. Results showed that pseudo-second-order reaction mechanism is well suited as compared to pseudo-first-order. The linear plots of t/q_t and t of pseudo-second-order shows the positive relation with $R^2 \leq 1$ [59] as compared to pseudo-first-order [82] (Figs. S10 and S11).

The results of the intraparticle diffusion model are divided into three-step adsorption processes and graphs plotted with q_t vs. $t^{0.5}$ are recorded for all the experimental systems. The diffusion in the meso- and micropores is represented by the two or multi-linear plots. The first step with a sharp slope confirms the external surface adsorption, the second step with a gradual slope demonstrate the intraparticle diffusion, and the third portion is the final step is the equilibrium stage where intraparticle diffusion starts to slow down due to extremely low adsorbate concentrations in the solution. The values of slope and intercept give an idea about the thickness of the boundary layer, that is, the larger the intercept, the greater is the boundary layer effect. The deviation of straight lines from the origin maybe because of the difference between the rate of mass transfer in the initial and final stages of adsorption. Further, such deviation of a straight line from the origin indicates that the pore diffusion is not the sole rate-controlling step [83] (Fig. S12).

6. Conclusion

Current research work is based on a synthesis of a very environmentally friendly gel composite based on GO and its functionalization with metal particles (Cu, Ag) for wastewater treatment. adsorption experiments were carried out at various parameters and %R percent removal was calculated. The results supported efficient removal of MG and Cd²⁺ ions (94% and 98%) by GO and functionalized GO

respectively. Kinetics study also favored pseudo-second-order along with best fit Langmuir and Freundlich isotherms for the experimental data. The three steps sorption process was noticed using the intraparticle diffusion model with an external mass transport mechanism (the Boyd plot). GO also possess antibacterial properties due to the efficient removal of *Staphylococcus aureus* species from wastewater. Hence, it is concluded that the functionalized GO had the highest multilayer adsorption capacity as (8.92, 8.08) compared to other adsorbents.

Recommendations

Graphene can be explored further by functionalizing with the efficient materials, that is, polymers, metals, copolymers, etc. and can be characterized using more accurate techniques for the evaluation of the capabilities of these micro materials. Derive the approaches for the synthesis of defect-free graphene that could yield more effective products upon functionalization. Eco-paving, the introduction of graphene entities in drug delivery and cancer treatments, and designing the devices based on graphene can harness the energy for a sustainable future.

Acknowledgments

We are grateful to the research laboratories of Fatima Jinnah Women University and Pakistan Environmental Protection Agency, Islamabad (Pak-EPA) to allow the steering of the current study.

References

- [1] M.S. Diallo, A. Street, R. Sustich, J. Duncan, N. Savage, Nanotechnology Applications for Clean Water: Solutions for Improving Water Quality, A volume in Micro and Nano Technologies, William Andrew, Norwich, New York, 2009.
- [2] M.J. Yoo, H.B. Park, Effect of hydrogen peroxide on properties of graphene oxide in Hummers Method, Carbon, 141 (2019) 515–522.
- [3] Office of Water, 'The Clean Water and Drinking Water Gap Analysis,' United States Environmental Protection Agency, Washington, D.C., 2002, p. 5.
- [4] K.E. Drexler, Engines of Creation: The Coming Era of Nanotechnology (1987, September 16). Retrieved January 19,

- Doubleday Publishers, London, 2019, Available at: http://edexler.com/p/06/00/EOC_Cover.html
- [5] F. Pendolino, N. Armata, Graphene Oxide in Environmental Remediation Process, Springer, Switzerland, 2017.
 - [6] G. Nabi, M. Ali, S. Khan, S. Kumar, The crisis of water shortage and pollution in Pakistan: risk to public health, biodiversity, and ecosystem, *Environ. Sci. Pollut. Res.*, 26 (2019) 10443–10445.
 - [7] A. Ahmed, I. Shafique, Perception of household in regards to water pollution: an empirical evidence from Pakistan, *Environ. Sci. Pollut. Res.*, 26 (2019) 8543–8551.
 - [8] K. He, G. Chen, G. Zeng, A. Chen, Z. Huang, J. Shi, T. Huang, M. Peng, L. Hu, Three-dimensional graphene supported catalysts for organic dyes degradation, *Appl. Catal., B*, 228 (2018) 19–28.
 - [9] M. Cametti, Z. Džolić, New frontiers in hybrid materials: noble metal nanoparticles – supramolecular gel systems, *Chem. Commun.*, 50 (2016) 8273–8286.
 - [10] N.H. Syed, J. Ahmad, N.A. Khan, M.A. Shafiq, N. Khan, A low-cost wastewater treatment unit for reducing the usage of fresh water at car wash stations in Pakistan, *Pak. J. Sci. Ind. Res.*, 62 (2019) 57–66.
 - [11] M.S. Abdel-Raouf, A.R.M. Abdul-Raheem, Removal of heavy metals from industrial waste water by biomass-based materials: a review, *J. Pollut. Eff. Contr.*, 5 (2017) 180, doi: 10.4172/2375-4397.1000180.
 - [12] T.T.N. Le, V.T. Le, M.U. Dao, Q.V. Nguyen, T.T. Vu, M.H. Nguyen, H.S. Le, Preparation of magnetic graphene oxide/chitosan composite beads for effective removal of heavy metals and dyes from aqueous solutions, *Chem. Commun.*, 206 (2019) 1337–1352.
 - [13] J. Tang, Y. Song, F. Zhao, S. Spinney, J. da Silva Bernardes, K.C. Tam, Compressible cellulose nanofibril (CNF) based aerogels produced via a bio-inspired strategy for heavy metal ion and dye removal, *Carbohydr. Polym.*, 208 (2019) 404–412.
 - [14] S. Nizamuddin, M.T.H. Siddiqui, N.M. Mubarak, H.A. Baloch, E.C. Abdullah, S.A. Mazari, G.J. Griffin, M.P. Srinivasan, A. Tanksale, Chapter 17 – Iron oxide nanomaterials for the removal of heavy metals and dyes from wastewater, S. Thomas, D. Pasquini, S.-Y. Leu, D.A. Gopakumar, Eds., *Nanoscale Materials in Water Purification: Micro and Nano Technologies*, Elsevier, Amsterdam, Netherlands, 2019, pp. 447–472.
 - [15] P.M. Dellamatrice, M.E. Silva-Stenico, L.A.B. de Moraes, M.F. Fiore, R.T.R. Monteiro, Degradation of textile dyes by cyanobacteria, *Braz. J. Microbiol.*, 48 (2017) 25–31.
 - [16] A.G. Varghese, S.A. Paul, M.S. Latha, Remediation of heavy metals and dyes from wastewater using cellulose-based adsorbents, *Environ. Chem. Lett.*, 17 (2019) 867–877.
 - [17] N. Minju, K. Venkat Swaroop, K. Haribabu, V. Sivasubramanian, P. Senthil Kumar, Removal of fluoride from aqueous media by magnesium oxide-coated nanoparticles, *Desal. Water Treat.*, 53 (2015) 2905–2914.
 - [18] S. Yu, X. Wang, X. Tan, X. Wang, Sorption of radionuclides from aqueous systems onto graphene oxide-based materials: a review, *Inorg. Chem. Front.*, 2 (2015) 593–612.
 - [19] S. Song, S. Zhang, S. Huang, R. Zhang, L. Yin, Y. Hu, X. Wang, A novel multi-shelled $\text{Fe}_3\text{O}_4/\text{MnO}_2$ hollow microspheres for immobilizing U(VI) and Eu(III), *Chem. Eng. J.*, 355 (2019) 697–709.
 - [20] G. Neeraj, S. Krishnan, P.S. Kumar, K.R. Shriaiswarya, V.V. Kumar, Performance study on sequestration of copper ions from contaminated water using newly synthesized high effective chitosan coated magnetic nanoparticles, *J. Mol. Liq.*, 214 (2016) 335–346.
 - [21] S. Yu, X. Wang, S. Yang, G. Sheng, A. Alsaedi, T. Hayat, X. Wang, Interaction of radionuclides with natural and manmade materials using XAFS technique, *Sci. China Chem.*, 60 (2017) 170–187.
 - [22] M. Montaña, A. Camacho, I. Serrano, R. Devesa, L. Mati, I. Vallés, Removal of radionuclides in drinking water by membrane treatment using ultrafiltration, reverse osmosis and electrodialysis reversal, *J. Environ. Radioact.*, 125 (2013) 86–92.
 - [23] V. Mikušová, O. Lukačovičová, E. Havránek, P. Mikuš, Radionuclide X-ray fluorescence analysis of selected elements in drug samples with 8-hydroxyquinoline preconcentration, *J. Radioanal. Nucl. Chem.*, 299 (2014) 1645–1652.
 - [24] S. Zhang, J. Li, X. Wang, Y. Huang, M. Zeng, J. Xu, In situ ion exchange synthesis of strongly coupled $\text{Ag}@\text{AgCl}/\text{g-C}_3\text{N}_4$ porous nanosheets as plasmonic photocatalyst for highly efficient visible-light photocatalysis, *ACS Appl. Mater. Interfaces*, 6 (2014) 22116–22125.
 - [25] V. Radchenko, J.W. Engle, J.J. Wilson, J.R. Maassen, F.M. Nortier, W.A. Taylor, M.E. Fassbender, Application of ion exchange and extraction chromatography to the separation of actinium from proton-irradiated thorium metal for analytical purposes, *J. Chromatogr. A*, 1380 (2015) 55–63.
 - [26] Y. Zou, X. Wang, Y. Ai, Y. Liu, J. Li, Y. Ji, X. Wang, Coagulation behavior of graphene oxide on nanocrystalline Mg/Al layered double hydroxides: batch experimental and theoretical calculation study, *Environ. Sci. Technol.*, 50 (2016) 3658–3667.
 - [27] H. Yu, B. Zhang, C. Bulin, R. Li, R. Xing, High-efficient synthesis of graphene oxide based on improved Hummers Method, *Sci. Rep.*, 6 (2016) 36143, doi: 10.1038/srep36143.
 - [28] N. Alipour, H. Namazi, Removing Paraquat and Nile blue from aqueous solution using double-oxidized graphene oxide coated by polydopamine nanocomposite, *Int. J. Environ. Sci. Technol.*, 16 (2019) 3203–3210.
 - [29] A. Murcia-Salvador, J.A. Pellicer, M.I. Fortea, V.M. Gómez-López, M.I. Rodríguez-López, E. Núñez-Delgado, J.A. Gabaldón, Adsorption of Direct Blue 78 using chitosan and cyclodextrins as adsorbents, *Polymers (Basel)*, 11 (2019) 1003, doi: 10.3390/polym11061003.
 - [30] K. Tewari, G. Singhal, R.K. Arya, Adsorption removal of Malachite green dye from aqueous solution, *Rev. Chem. Eng.*, 34 (2018) 427–453.
 - [31] M.S. Tizo, L.A.V. Blanco, A.C.Q. Cagas, B.R.B.D. Cruz, J.C. Encoy, J.V. Gunting, V.I.F. Mabayo, Efficiency of calcium carbonate from eggshells as an adsorbent for cadmium removal in aqueous solution, *Sustainable Environ. Res.*, 28 (2018) 326–332.
 - [32] P.V. Kamat, Graphene-based nanoarchitectures. Anchoring semiconductor and metal nanoparticles on a two-dimensional carbon support, *J. Phys. Chem. Lett.*, 1 (2009) 520–527.
 - [33] P. Cadden-Zimansky, M. Shinn, G.T. Myers, Y. Chu, M.J. Dalrymple, H.C. Travaglini, Formation of the $n = 0$ Landau level in hybrid graphene, *J. Phys. Commun.*, 2 (2018) 051001.
 - [34] I.A. Ovid'ko, Metal-graphene nanocomposites with enhanced mechanical properties: a review, *Rev. Adv. Mater. Sci.*, 38 (2014) 190–200.
 - [35] A. Dimiev, D.V. Kosynkin, L.B. Alemany, P. Chaguine, J.M. Tour, Pristine graphite oxide, *J. Am. Chem. Soc.*, 134 (2012) 2815–2822.
 - [36] A.A. Alqadami, M. Naushad, Z.A. AlOthman, M. Alsuhybani, M. Algamdi, Excellent adsorptive performance of a new nanocomposite for removal of toxic Pb(II) from aqueous environment: adsorption mechanism and modeling analysis, *J. Hazard. Mater.*, 389 (2020) 121896, doi: 10.1016/j.jhazmat.2019.121896.
 - [37] T. Ahmed, S. Imdad, K. Yaldrum, S.M. Raza, Awareness and attitude about nanotechnology in Pakistan, *J. Nano Res.*, 7 (2015) 44–51.
 - [38] V. Modi, S. Akst, D. Davison, 1715: acute cadmium toxicity causing multisystem organ failure, *J. Respir. Crit. Care Sleep Med.*, 47 (2019) 831, doi: 10.1097/01.ccm.0000552454.38387.20.
 - [39] S. Chehreh Chelgani, M. Rudolph, R. Kratzsch, D. Sandmann, J. Gutzmer, A review of graphite beneficiation techniques, *Miner. Process. Extr. Metall. Rev.: Int. J.*, 37 (2016) 58–68.
 - [40] A. George, R. Ganesan, T. Thangeeswari, Redox deposition of manganese oxide nanoparticles on graphite electrode by immersion technique for electrochemical super capacitors, *Indian J. Sci. Technol.*, 9 (2016) 85782, doi: 10.17485/ijst/2016/v9i1/85782.
 - [41] J.H. Kang, T. Kim, J. Choi, J. Park, Y.S. Kim, M.S. Chang, C.R. Park, Hidden second oxidation step of Hummers Method, *Chem. Mater.*, 28 (2016) 756–764.
 - [42] D. Liu, Q. Bian, Y. Li, Y. Wang, A. Xiang, H. Tian, Effect of oxidation degrees of graphene oxide on the structure and

- properties of poly(vinyl alcohol) composite films, *Compos. Sci. Technol.*, 129 (2016) 146–152.
- [43] P. Feicht, J. Biskupek, T.E. Gorelik, J. Renner, C.E. Halbig, M. Maranska, S. Eigler, Brodie's or Hummers' method: oxidation conditions determine the structure of graphene oxide, *Chem. Eur. J.*, 25 (2019) 8955–8959.
- [44] B. Paulchamy, G. Arthi, B.D. Lignesh, A simple approach to stepwise synthesis of graphene oxide nanomaterial, *J. Nanomed. Nanotechnol.*, 6 (2015) 1000253, doi: 10.4172/2157-7439.1000253.
- [45] W. Chen, L. Yan, Preparation of graphene by a low-temperature thermal reduction at atmosphere pressure, *Nanoscale*, 2 (2010) 559–563.
- [46] S. Basu, S. Hazra, Graphene–noble metal nano-composites and applications for hydrogen sensors, *Carbon*, 3 (2017) 29, doi: 10.3390/c3040029.
- [47] Y. Tian, F. Wang, Y. Liu, F. Pang, X. Zhang, Green synthesis of silver nanoparticles on nitrogen-doped graphene for hydrogen peroxide detection, *Electrochim. Acta*, 146 (2014) 646–653.
- [48] K.T. Dissanayake, W. Rohini de Silva, A. Kumarasinghe, K.M. Nalin de Silva, Synthesis of graphene and graphene oxide based nanocomposites and their characterization, *SAITM*, 1 (2014) 75–78.
- [49] H. Chang, H. Wu, Graphene-based nanocomposites: preparation, functionalization, and energy and environmental applications, *Energy Environ. Sci.*, 6 (2013) 3483–3507.
- [50] B. Zahed, H. Hosseini-Monfared, A comparative study of silver-graphene oxide nanocomposites as a recyclable catalyst for the aerobic oxidation of benzyl alcohol: support effect, *Appl. Surf. Sci.*, 328 (2015) 536–547.
- [51] Q. Bao, D. Zhang, P. Qi, Synthesis and characterization of silver nanoparticle and graphene oxide nanosheet composites as a bactericidal agent for water disinfection, *J. Colloid Interface Sci.*, 360 (2011) 463–470.
- [52] A.A. Velayati, P. Farnia, Nontuberculous Mycobacteria (NTM): Microbiological, Clinical and Geographical Distribution, Academic Press, London, 2019.
- [53] L. Shi, J. Chen, L. Teng, L. Wang, G. Zhu, S. Liu, L. Ren, The antibacterial applications of graphene and its derivatives, *Small*, 12 (2016) 4165–4184.
- [54] Y. Zhu, S. Murali, W. Cai, X. Li, J. Suk, J.R. Potts, R.S. Ruoff, Graphene and graphene oxide: synthesis, properties, and applications, *Adv. Mater.*, 22 (2010) 3906–3924.
- [55] J. Hwang, T. Yoon, S.H. Jin, J. Lee, T.S. Kim, S.H. Hong, S. Jeon, Enhanced mechanical properties of graphene/copper nanocomposites using a molecular-level mixing process, *Adv. Mater.*, 25 (2013) 6724–6729.
- [56] S. Chaiyakun, N. Witit-Anun, N. Nuntawong, P. Chindaudom, S. Oaew, C. Kedkeaw, P. Limsuwan, Preparation and characterization of graphene oxide nanosheets, *Procedia Eng.*, 32 (2012) 759–764.
- [57] D.W. Lee, L.V. de Los Santos, J.W. Seo, L.L. Felix, A.D. Bustamante, J.M. Cole, C.H.W. Barnes, The structure of graphite oxide: investigation of its surface chemical groups, *J. Phys. Chem.*, 114 (2010) 5723–5728.
- [58] J. Gao, F. Bao, L. Feng, K. Shen, Q. Zhu, D. Wang, C. Yan, Functionalized graphene oxide modified polysebacic anhydride as drug carrier for levofloxacin controlled release, *RSC Adv.*, 1 (2011) 1737–1744.
- [59] M.S. Eluyemi, M.A. Eleruja, A.V. Adedeji, B. Olofinjana, O. Fasakin, O.O. Akinwunmi, O.O. Ilori, A.T. Famojuro, S.A. Ayinde, E.O.B. Ajayi, Synthesis and characterization of graphene oxide and reduced graphene oxide thin films deposited by spray pyrolysis method, *Graphene*, 5 (2016) 143–154.
- [60] L. Shahriary, A.A. Athawale, Graphene oxide synthesized by using modified hummers approach, *Int. J. Renewable Energy Environ. Eng.*, 2 (2014) 58–63.
- [61] C.H. Manaratne, S.R.D. Rosa, I.R.M. Kottegoda, XRD-HTA, UV visible, FTIR and SEM interpretation of reduced graphene oxide synthesized from high purity vein graphite, *Mater. Sci. Res. India*, 14 (2017) 19–30.
- [62] S. Thakur, N. Karak, Alternative methods and nature-based reagents for the reduction of graphene oxide: a review, *Carbon*, 94 (2015) 224–242.
- [63] W.W. Mhike, H.J. Kruger, D. Lombaard, Characterization of commercial expandable graphite fire retardants, *Thermochim. Acta*, 584 (2014) 8–16.
- [64] D.C. Weindorf, S. Chakraborty, Portable X-ray fluorescence spectrometry analysis of soils, *Soil Sci. Soc. Am. J.*, 84 (2020) 1384–1392.
- [65] Z. Sofer, O. Jankovský, P. Šimek, L. Soferová, D. Sedmidubský, M. Pumera, Highly hydrogenated graphene via active hydrogen reduction of graphene oxide in the aqueous phase at room temperature, *Nanoscale*, 6 (2014) 2153–2160.
- [66] J. Liu, H. Yan, M.J. Reece, K. Jiang, Toughening of zirconia/alumina composites by the addition of graphene platelets, *J. Eur. Ceram. Soc.*, 32 (2012) 4185–4193.
- [67] E. Aliyev, V. Filiz, M. Khan, Y.J. Lee, C. Abetz, V. Abetz, Structural characterization of graphene oxide: Surface functional groups and fractionated oxidative debris, *Nanomaterials*, 9 (2019) 1180, doi: 10.3390/nano9081180.
- [68] H. Pardo, R. Faccio, F.M. Araújo-Moreira, O.F. De Lima, A.W. Mombrú, Synthesis and characterization of stable room temperature bulk ferromagnetic graphite, *Carbon*, 44 (2006) 565–569.
- [69] A.U. Liyanage, E.U. Ikhuria, A.A. Adenuga, V.T. Remcho, M.M. Lerner, Synthesis and characterization of low-generation polyamidoamine (PAMAM) dendrimer-sodium montmorillonite (Na-MMT) clay nanocomposites, *Inorg. Chem.*, 52 (2013) 4603–4610.
- [70] T.S. Sreepasad, S.M. Maliyekkal, K.P. Lisha, T. Pradeep, Reduced graphene oxide–metal/metal oxide composites: facile synthesis and application in water purification, *J. Hazard. Mater.*, 186 (2011) 921–931.
- [71] M. Rafi, B. Samiey, C.-H. Cheng, Study of adsorption mechanism of Congo red on graphene oxide/PAMAM nanocomposite, *Materials*, 11 (2018) 496, doi: 10.3390/ma11040496.
- [72] D. Wang, L. Liu, X. Jiang Adsorption and removal of Malachite green from aqueous solution using magnetic cyclodextrin-graphene oxide nanocomposites as adsorbents, *Colloids Surf., A*, 466 (2015) 166–173.
- [73] S. Debnath, A. Maity, K. Pillay, Impact of process parameters on removal of Congo red by graphene oxide from aqueous solution, *J. Environ. Chem. Eng.*, 2 (2014) 260–272.
- [74] H. Hou, R. Zhou, P. Wu, L. Wu, Removal of Congo red dye from aqueous solution with hydroxyapatite/chitosan composite, *Chem. Eng. J.*, 211 (2012) 336–342.
- [75] A.C. Obreja, D. Cristea, R. Gavrilă, V. Schiopu, A. Dinescu, M. Danila, F. Comanescu, Isocyanate functionalized graphene/P3HT based nanocomposites, *Appl. Surf. Sci.*, 276 (2013) 458–467.
- [76] W. Xing, G. Lalwani, I. Rusakova, B. Sitharaman, Degradation of graphene by hydrogen peroxide, *Part. Part. Syst. Char.*, 31 (2014) 745–750.
- [77] Z. Aly, A. Graulet, N. Scales, T. Hanley, Removal of aluminium from aqueous solutions using PAN-based adsorbents: characterisation, kinetics, equilibrium and thermodynamic studies, *Environ. Sci. Pollut. Res.*, 21 (2014) 3972–3986.
- [78] I. Yin, J. Zhang, I.S. Zhao, M.L. Mei, Q. Li, C.H. Chu, The antibacterial mechanism of silver nanoparticles and its application in dentistry, *J. Nanomedicine*, 15 (2020) 2555–2562.
- [79] H. Kim, S.-O. Kang, S.G. Park, H.S. Park, Adsorption isotherms and kinetics of cationic and anionic dyes on three-dimensional reduced graphene oxide macrostructure, *J. Ind. Eng. Chem.*, 21 (2015) 1191–1196.
- [80] P. Ramachandran, R. Vairamuthu, S. Ponnusamy, Adsorption isotherms, kinetics, thermodynamics and desorption studies of reactive Orange 16 on activated carbon derived from *Ananas comosus* (L.) carbon, *J. Eng. Appl. Sci.*, 6 (2011) 15–26.
- [81] R.S. Krishna, J. Mishra, S.K. Das, S.M. Mustakim, An overview of current research trends on graphene and its applications, *World Sci. News.*, 132 (2019) 206–219.

- [82] A. Abbas, A.M. Al-Amer, T. Laoui, M.J. Al-Marri, M.S. Nasser, M. Khraisheh, M.A. Atieh, Heavy metal removal from aqueous solution by advanced carbon nanotubes: critical review of adsorption applications, *Sep. Purif. Technol.*, 157 (2016) 141–161.
- [83] C. McGladdery, D.C. Weindorf, S. Chakraborty, B. Li, L. Paulette, D. Podar, B. Duda, Elemental assessment of vegetation via portable X-ray fluorescence (PXRF) spectrometry, *J. Environ. Manage.*, 210 (2018) 210–225.

Table S1
XRF results composition indicated as %ages

No.	Metals	G(c)	GO(c)	AgGO(c)	CuGO(c)
1.	Cu	0.44	–	0.12	51.52
2.	Ag	–	0.07	60.15	–
3.	Ti	3.66	0.09	0.12	–
4.	Co	–	–	–	–
5.	Cr	–	–	–	–
6.	Fe	60.85	–	0.23	–
7.	Mn	1.44	98.66	38.07	47.91
8.	Pd	6.22	0.15	0.25	0.08
9.	Si	6.97	0.45	0.57	0.37
10.	Zn	4.31	–	0.04	–
11.	S	1.52	0.46	0.04	0.05
12.	W	–	–	–	0.07
13.	Au	2.04	–	–	–
14.	Nb	0.67	0.02	–	–
15.	Ni	1.55	–	–	–
16.	Se	–	–	0.05	–
17.	Zr	1.30	–	–	–
18.	Sb	2.49	–	0.20	–
19.	Sn	2.12	0.11	0.16	–
20.	Cd	–	–	–	–
21.	Mo	0.46	–	–	–
22.	As	3.55	–	–	–
%age	100	100	100	100	100

Appendix A: Supplementary data



Fig. S1. Catalase test.

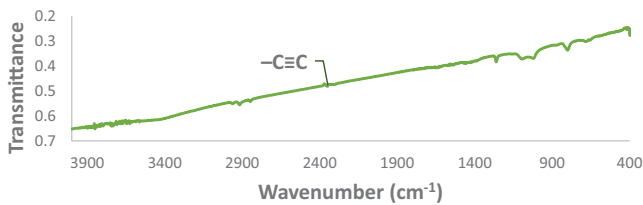


Fig. S2. FTIR spectra of graphite cells.

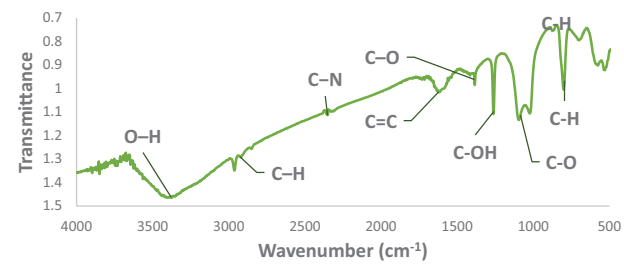


Fig. S3. FTIR spectra of graphene oxide-cells.

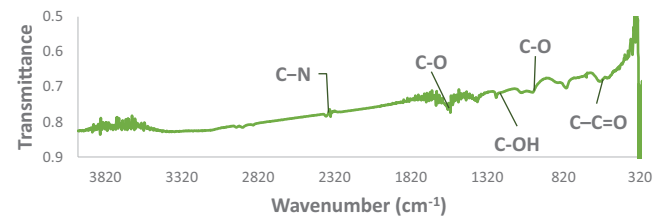


Fig. S4. FTIR spectra of AgGO(c).

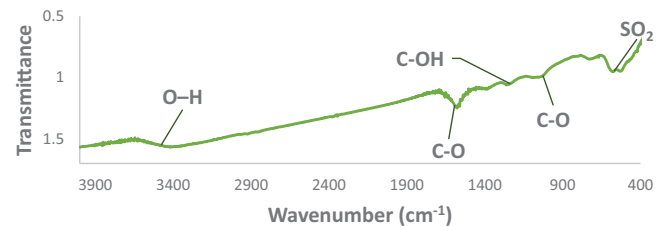


Fig. S5. FTIR spectra of CuGO(c).

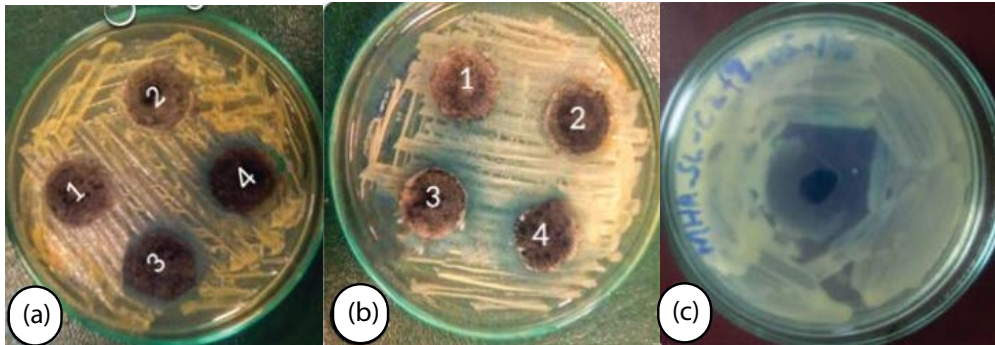


Fig. S6. Anti-microbial (a) AgGO(c), (b) CuGO(c) and (c) GO(c).

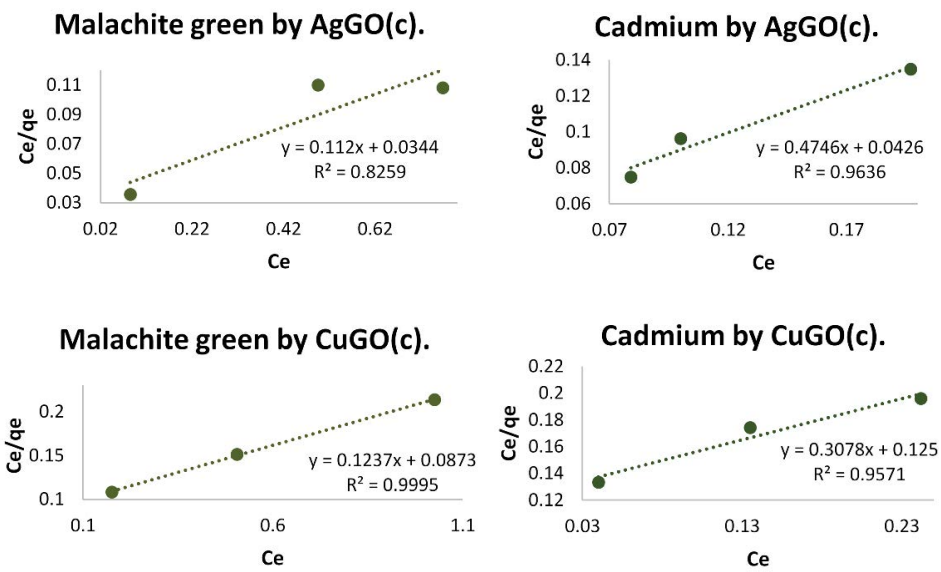


Fig. S7. Langmuir adsorption model.

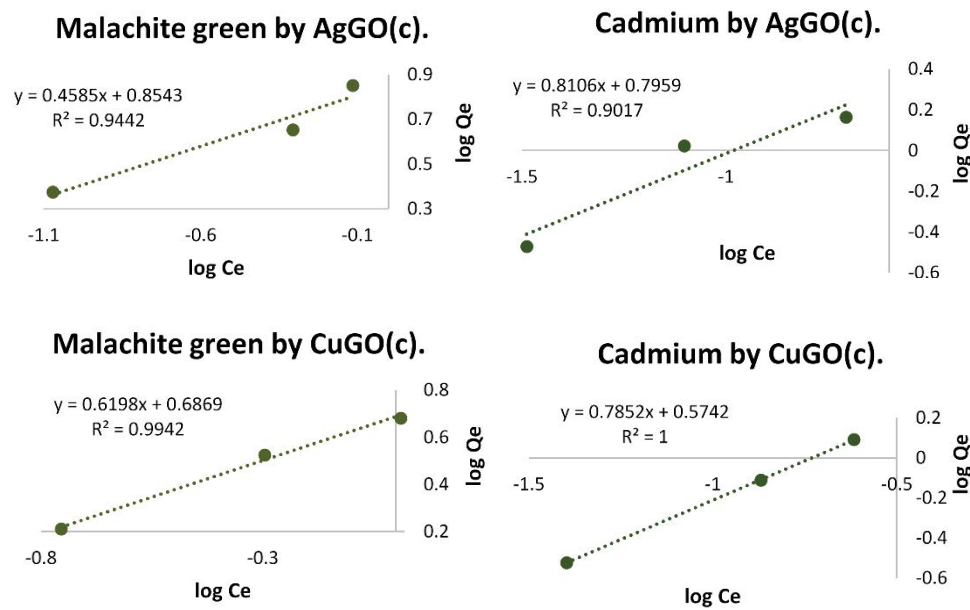


Fig. S8. Freundlich adsorption model.

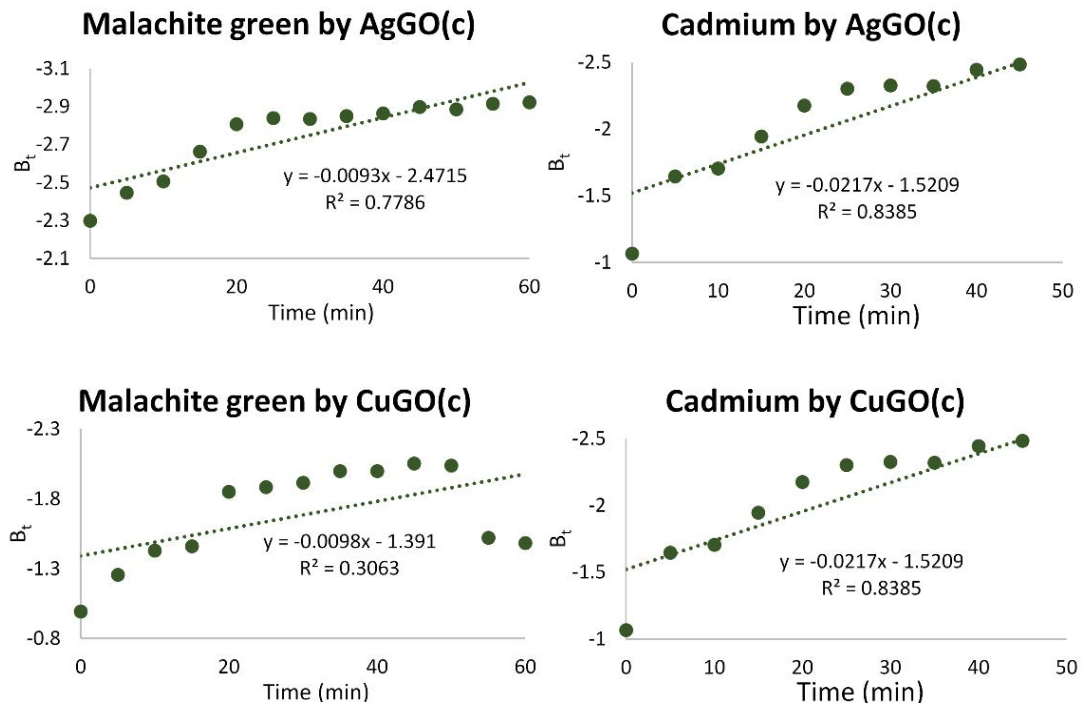


Fig. S9. Boyd plot.

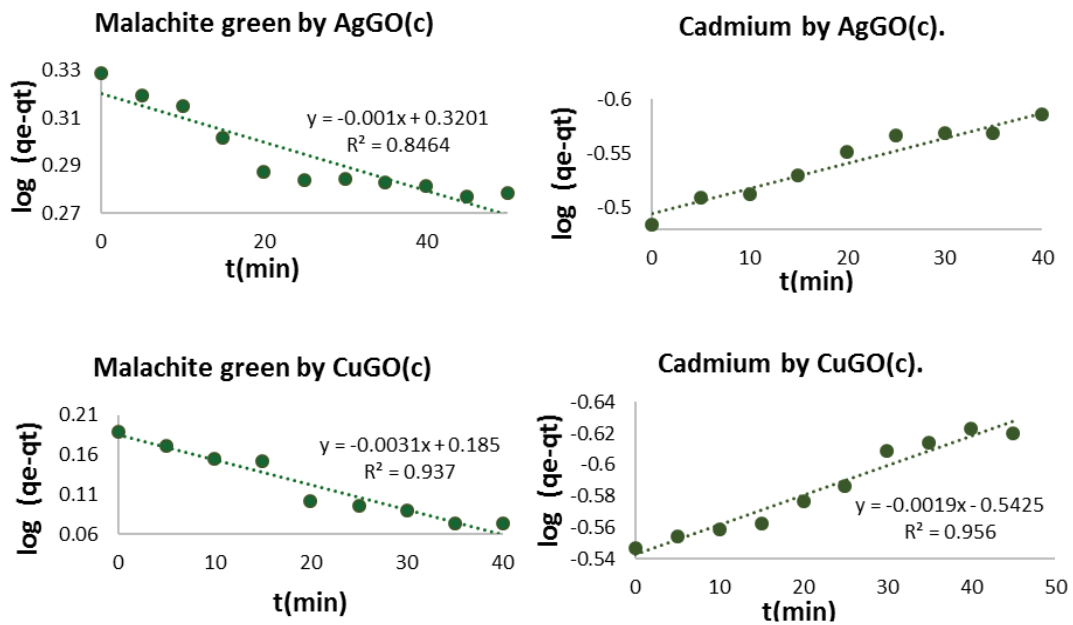


Fig. S10. Pseudo-first-order kinetics.

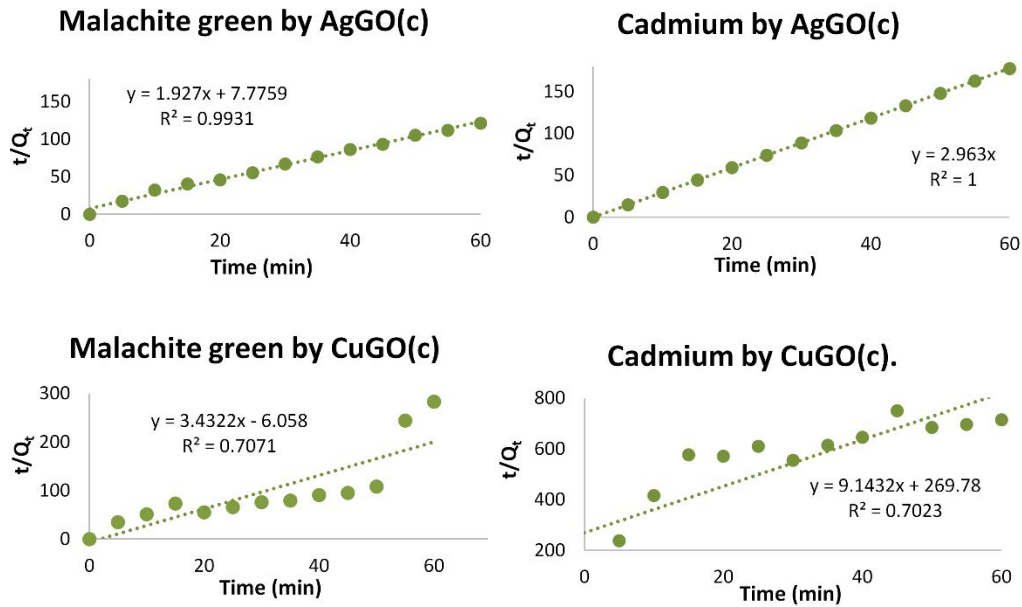


Fig. S11. Pseudo-second-order kinetics.

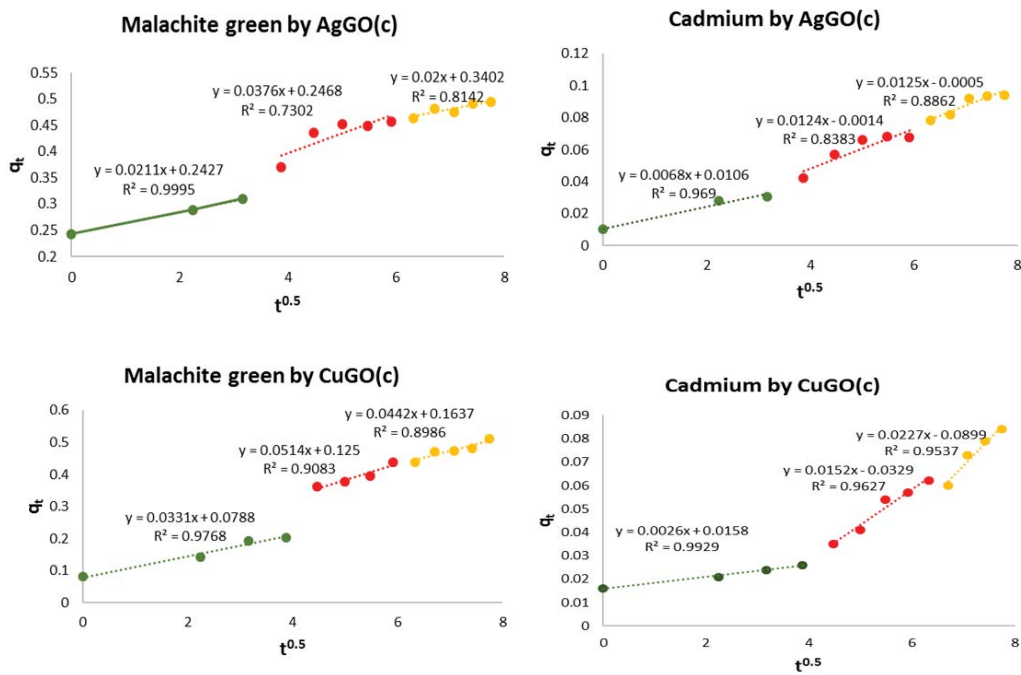


Fig. S12. Intraparticle adsorption model.